Characterization of ZnE (E = S, Se, or Te) Materials Synthesized Using Silylated Chalcogen Reagents in Mesoporous MCM-41

Elizabeth A. Turner,[†] Harald Rösner,[‡] Dieter Fenske,[‡] Yining Huang,*[,†] and John F. Corrigan*[,†]

Department of Chemistry, The University of Western Ontario, London, Ontario N6A 5B7, Canada, and Institut für Nanotechnologie, Forschungszentrum Karlsruhe GmbH, 76344 Eggenstein-Leopoldshafen, Germany

Received: January 8, 2006; In Final Form: May 9, 2006

The binary materials ZnS, ZnSe, and ZnTe have been successfully prepared within the mesoporous framework of MCM-41 at room temperature through the use of silylated chalcogen reagents. Postsynthesis grafting of ethylenediamine facilitates the complexation of anhydrous zinc acetate to the pore surface via a ligand exchange process between monodentate 3,5-lutidine ligands and the anchored chelating moiety. Coordinated zinc acetate readily reacts with $E(SiMe_3)_2$ (E = S, Se, or Te), thereby encapsulating zinc chalcogenides in the mesoporous channels. ZnE−MCM-41 materials have been characterized by EDX analysis, nitrogen sorption analysis, and Raman, UV−vis, and solid-state NMR spectroscopy. The observed blue shift in the absorption maximum is in agreement with the expected quantum confinement of these materials given the nanometer dimensions of the mesoporous architecture of the silicate host.

Introduction

Trimethylsilyl chalcogenolate or chalcogenide reagents [RE-$SiMe_3$ and $E(SiMe_3)_2$; R = alkyl, aryl, or ferrocenyl] are convenient precursors for the delivery of a chalcogenide or chalcogenolate source. The highly reactive nature of these silylated chalcogen reagents can be utilized in the pursuit of metal−chalcogen materials and has thus led to the formation of structurally characterized clusters[1] and nanoparticles.[2] Silylated chalcogen reagents are an efficient delivery source of E^{2-} and RE^- as they provide homogeneous reaction conditions in addition to reacting readily with both transition and main group metal salts, where either acetates or halide salts have been successfully employed.[3] The formation of M−E bonding interactions is promoted by the thermodynamically favored generation and elimination of the corresponding trimethylsilane. The ability to perform these syntheses using a surface-modified mesoporous host would permit a general route to functionalized mesoporous materials.

The field of ordered mesoporous materials has grown considerably since the discoveries of MCM-41[4] and SBA-15.[5] The distinctive hexagonal array of mesoporous channels offers a viable route to inclusion chemistry within a unique chemical environment. Over the past decade, these siliceous mesoporous frameworks have been developed as nanoreactors in which catalysis,[6] polymerization,[7] and adsorption and separation[8] of toxic species have been successfully demonstrated. Of particular interest is the encapsulation of nanoparticle species within MCM-41 and SBA-15. The nanometer-sized pore is ideal for the growth and inclusion of nanoparticle semiconductor materials, where the walls of the confining environment hinder particle−particle interactions, thus preventing cluster agglomeration.

In this vein, the inclusion of semiconductor species within MCM-41 and SBA-15 has been the focus of intense research in recent years. As such, Si,[9] Ge,[10] III−V,[11] metal oxide,[12] Cd_3P_2,[13] and II−VI[14−16] nanomaterials have been both synthesized and confined to the mesoporous environment. Despite the immense interest in this area, perhaps the most comprehensively investigated class of semiconductors is that of II−VI materials. The multitude of synthetic approaches that have been utilized in developing ME (M = Zn or Cd and E = S, Se, or Te) nanoparticles within MCM-41 and SBA-15 has been highlighted in recent reviews.[17] The majority of these studies have investigated CdS[14] and CdSe,[15] with a handful of examples investigating the synthesis of ZnS.[16] Generally when ME nanoparticles are being synthesized within the framework, there are two major approaches to initially incorporating the metal within the hexagonal array. In one method, the ionic nature of the host environment is exploited, allowing desired metal cations to be introduced into the framework structure via ion exchange.[14a−e,15a,16a−c] Alternatively, the host material can undergo organic functionalization with an appropriate alkoxysilane, a procedure that has been thoroughly studied in the literature.[18] The presence of an organic thiol or ethylenediamine moiety can be used to adsorb the preferred metal salt.[14f−k,16d−f] Upon encapsulation of the metal within the framework, binary chalcogenide materials are typically formed using H_2E (E = S or Se),[14b−g,15a,16a−e] although Na_2S,[14a,i−k,16f] Na_2SeO_3,[15c] and thiourea[14l] have also been successfully used as chalcogen sources.

Anhydrous zinc acetate can be successfully anchored to the surface of MCM-41 through organic functionalization of the pore wall[12a,16d] and will readily react with bis(trimethylsilyl)-chalcogenide [$E(SiMe_3)_2$] to form M−E bonds. Apart from being an alternative approach to ZnE materials in MCM-41, this route offers relatively simple handling procedures while accessing the higher congeners (Se and Te) of the ZnE series (Scheme 1). Herein, we report the characterization of ZnS, ZnSe, and ZnTe materials obtained using $E(SiMe_3)_2$, demonstrating

* To whom correspondence should be addressed. Phone: (519) 661-2111, ext. 86387 (J.F.C.); (519) 661-2111, ext. 86384 (Y.H.). Fax: (519) 661-3022.

[†] The University of Western Ontario.

[‡] Forschungszentrum Karlsruhe GmbH.

10.1021/jp060135c CCC: $33.50
Published on Web 07/29/2006

SCHEME 1: Proposed Synthetic Scheme for the Synthesis of Binary ZnE Materials in MCM-41[a]

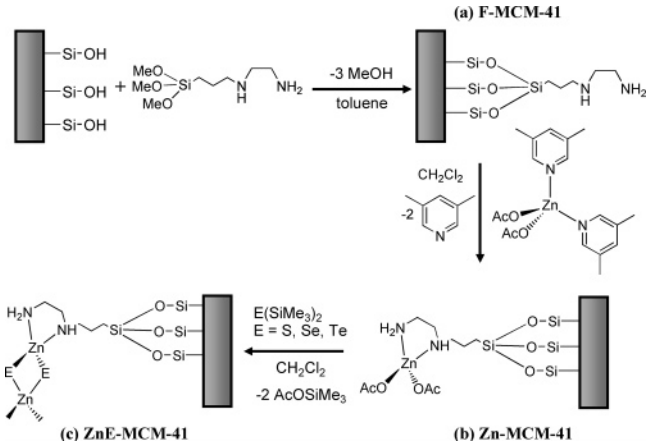

[a] (a) Functionalization of MCM-41 with TPED (F−MCM-41), (b) coordination of Zn(II) to the pore surface via the chelate effect (Zn−MCM-41), and (c) synthesis of ZnE materials through the use of silylated chalcogenide reagents (ZnE−MCM-41).

the general utility of silylated chalcogen reagents for delivery of E^{2-} to metal centers within the interior surfaces of MCM-41, including the first account of formation of ZnSe and ZnTe within MCM-41. EDX analysis, nitrogen sorption analysis, and Raman, UV−vis, and solid-state NMR spectroscopy have been used to investigate the formation of the binary complexes from molecular precursors.

Experimental Section

Materials. All synthetic procedures and manipulations were performed under an inert nitrogen atmosphere using standard Schlenk techniques and gloveboxes, unless otherwise noted. Toluene was purchased from Caledon and was dried and collected using an MBraun MB-SPS solvent purification system with a tandem activated alumina/activated copper redox catalyst.[19] Dichloromethane (EMD) and chloroform-*d* (Cambridge Isotope Laboratories) were dried and distilled over P_2O_5. 3,5-Lutidine (Aldrich) was dried and distilled over sodium metal. Cetyltrimethylammonium bromide, *N*-[3-(trimethoxysilyl)propyl]ethylenediamine (TPED), hexadecane, and anhydrous zinc acetate (99.99%) were purchased from Aldrich. N-Brand sodium silicate (28.7% SiO_2) was purchased from PQ Corp. Concentrated sulfuric acid was obtained from Caledon. MCM-41[4] (synthesized under hydrothermal conditions) and the $E(SiMe_3)_2$ reagents (E = S, Se, or Te)[20] were synthesized according to literature procedures.

Functionalization of MCM-41 (F−MCM-41). MCM-41 (4.0 g) that had been calcined at 540 °C for 12 h was degassed at 10^{-3} Torr for 30 min and then suspended in dry toluene (100 mL). Hexadecane (0.5 mL) was added to the suspension to be used as an internal standard to monitor the functionalization process via GC−MS. *N*-[3-(Trimethoxysilyl)propyl]ethylenediamine (4.0 mL, 18.3 mmol) was added to the suspension such that the ratio of MCM-41 to TPED was 1:1 (m:v). The resulting mixture was allowed to reflux for 96 h. The solid was then isolated via inert atmosphere filtration and washed repeatedly with CH_2Cl_2 (3 × 50 mL). The white solid was dried under vacuum (10^{-3} Torr) at 105 °C for 2 days.

Zinc−MCM-41 (Zn−MCM-41). Zinc acetate (0.92 g, 5 mmol) was dissolved in CH_2Cl_2 (30 mL) and 2.5 equiv of 3,5-lutidine (1.43 mL, 12.5 mmol) and the mixture allowed to stir for 30 min, producing a clear and colorless solution of (3,5-lutidine)$_2$Zn(OAc)$_2$.[21] The solution was then added to a suspension of F−MCM-41 (2.0 g) in CH_2Cl_2 (30 mL) and toluene (0.5 mL; internal standard), where the ratio of F−MCM-41 to zinc complex was 1:1 (m:m). The resulting mixture was allowed to stir at room temperature for 96 h. The solid was then isolated via inert atmosphere filtration, washed repeatedly with CH_2Cl_2 (3 × 30 mL), and dried under vacuum (10^{-3} Torr) for several hours.

Zinc Sulfide−MCM-41 (ZnS−MCM-41). Zn−MCM-41 (0.10 g) was suspended in CH_2Cl_2 (10 mL) and toluene (0.05 mL; internal standard). $S(SiMe_3)_2$ (0.05 mL, 0.24 mmol) was added to the suspension and the mixture allowed to stir for 24 h at room temperature. The white solid was isolated via centrifugation in a nitrogen glovebox, washed with CH_2Cl_2 (2 × 5 mL), and dried under vacuum (10^{-3} Torr).

Zinc Selenide−MCM-41 (ZnSe−MCM-41). Zn−MCM-41 (0.10 g) was suspended in CH_2Cl_2 (10 mL) and toluene (0.05 mL; internal standard). $Se(SiMe_3)_2$ (0.05 mL, 0.23 mmol) was added to the suspension and the mixture allowed to stir for 24 h at room temperature. With continual stirring, the color of the suspension changed from white to pale yellow. The yellow solid was isolated via centrifugation in a nitrogen glovebox, washed with CH_2Cl_2 (2 × 5 mL), and dried under vacuum (10^{-3} Torr). The solid was stored in a glovebox as long-term exposure to air resulted in decomposition of the sample, leading to a darkening of the sample color.

Zinc Telluride−MCM-41 (ZnTe−MCM-41). Zn−MCM-41 (0.10 g) was suspended in CH_2Cl_2 (10 mL) and toluene (0.05 mL; internal standard). $Te(SiMe_3)_2$ (0.05 mL, 0.23 mmol) was added to the suspension and allowed to stir for 5 min at room temperature. Immediately after the addition, the color of the suspension changed from white to red-orange. The red-orange solid was isolated via centrifugation in a nitrogen glovebox, washed with CH_2Cl_2 (2 × 5 mL), and dried under vacuum (10^{-3} Torr). The solid was stored in a glovebox as short-term exposure to air resulted in rapid decomposition of the sample, leading to a darkening of the sample color.

Characterization. Powder X-ray diffraction (PXRD) patterns were obtained using a Rigaku diffractometer with a Co Kα radiation source ($\lambda = 1.799260$ Å). Thermogravimetric analyses (TGA) were carried out with a Mettler Toledo TGA/SDTA 851[e] device using a heating rate of 20 °C/min between 25 and 1000 °C. Surface area measurements were taken using a Micromeritics ASAP 2020 analyzer, in which the adsorption and desorption isotherms were obtained at 77 K after each sample was dehydrated at 105 °C for 10 h. The zinc chalcogenide−MCM-41 samples were dehydrated at 40 °C for 5 h prior to analysis. The surface area was calculated from the linear part of the BET plot while pore size distributions were estimated using the 4V/A approximation. Ultraviolet−visible (UV−vis) absorption spectra were recorded on an Ocean Optics SD2000 UV−vis fiber optic spectrometer equipped with a Mini-D2T light source and a UV2/OFLV-4 detector. The spectra were obtained as a mineral oil mull between two quartz plates. Luminescence measurements were taken using a Photo Technology International fluorimeter equipped with an LPS 220B lamp power supply and a model 814 photomultiplier detection system. The spectra were obtained for a suspension in degassed water. Photoluminescence and photoluminescence excitation spectra of ZnSe−MCM-41 were obtained by irradiation at 275 and 437 nm, respectively. The progress of each reaction was monitored using a Varian CP-3800 gas chromatograph coupled to a Varian Saturn 2000 GC/MS/MS mass spectrometer used as the detector. Raman spectra were obtained using a Bruker RFS 100/S spectrometer with a

resolution of 4 cm^{-1}. Solid-state ^{13}C cross-polarization magic-angle spinning (CP-MAS) and ^{29}Si MAS NMR spectra were recorded at operating frequencies of 100.46 and 79.36 MHz, respectively, using a Varian/Chemagnetic Infinitypulse 400 wide bore spectrometer at a field strength of 9.4 T. Solution ^{1}H NMR spectra were recorded on a Varian Mercury 400 spectrometer with an operating frequency of 400.09 MHz. Energy-dispersive X-ray (EDX) analyses were carried out by B. Hart at Surface Science Western (The University of Western Ontario). A Quartz Xone EDX analysis system coupled to a Leo 440 SEM equipped with a Gresham light element detector was used to obtain semiquantitative analysis of Zn, S, Se, and Te. Analyses were carried out using a 25 kV electron beam rastered over 100 μm $\times$ 100 μm areas and repeated to ensure reproducibility. Samples for high-resolution transmission electron microscopy (HRTEM) were obtained by dispersing the solid in CH_2Cl_2 and dropping these dilute suspensions on gold-plated grids, allowing the excess solvent to evaporate. TEM investigations were performed in a Philips Tecnai F20 ST instrument operated at 200 kV. The TEM was equipped with an EDAX energy-dispersive X-ray SiLi detector with a S-UTW (super-ultra-thin window). EDX analyses were carried out in the STEM mode with a HAADF (high-angle annular dark field) detector using a nanometer-sized probe (1 nm spot size for the presented measurements). Use was made of an analytic double tilt holder (Philips). High-resolution micrographs were taken with a 1K $\times$ 1K CCD camera and analyzed with Digital Micrographs, version 3.5.2 (Gatan Company), in performing fast Fourier transformations (FFT).

Results and Discussion

Synthesis and Characterization of F−MCM-41. The synthesis of F−MCM-41 is slightly modified from that of the original procedure,[12a] thus ultimately leading to maximum loading conditions while maintaining an appreciable surface area for further synthetic manipulations. The original method requires a 1:5 (m:v) ratio of MCM-41 to *N*-[3-(trimethoxysilyl)propyl]-ethylenediamine (TPED) while allowing the mixture to reflux for 10 h. It has also been reported that the addition of a small amount of water to the MCM-41 sample promotes surface hydrolysis, consequently leading to an increased population of surface silanol groups and fundamentally contributing to increased surface coverage of a desired organic moiety.[22]

The extent of functionalization can easily be monitored by GC−MS where an internal standard (hexadecane) that is nonreactive to the pore structure is added to the reaction mixture. By periodically analyzing the mother liquor from the reaction, we determined the quantity of TPED remaining in the reaction solution. It is observed that after being refluxed for a period of 12 h, F−MCM-41 materials formed using a 1:1 MCM-41:TPED ratio gave the highest percent loading (19%) in the absence of water versus a 1:0.25 ratio which yielded materials having a percent coverage of 14%. GC−MS analysis of reaction solutions indicates that after a 12 h period, TPED remains 1:1 with the mixture while it is completely consumed in 12 h using a ratio of 1:0.25 or 1:0.5. Increasing to 2 equiv of TPED did not lead to greater surface coverage of ethylenediamine as determined by TGA. Using a ratio of 1:0.25, however, led to a larger surface area (868 m^2/g) versus the functionalized material prepared using a ratio of 1:1 (598 m^2/g). The maximum surface coverage to be obtained from a 1:1 ratio of MCM-41 to TPED can also be determined by analyzing the reaction solution at specified time intervals. Thus, an aliquot of mother liquor is analyzed by GC−MS to monitor the change of TPED to hexadecane over the refluxing period, while the corresponding solid sample from the aliquot is examined by TGA to observe an increase in loading over time. The limit of functionalization is thus reached when there is no longer consumption of TPED (as determined by GC−MS) coupled with a nonfluctuating percent coverage. It is observed that extensive loading of the ethylenediamine moiety is achieved within the first hour of reflux where the ratio of TPED to hexadecane dramatically decreases from 9.3 to 3.6. This is also reflected in the TGA trace where there is 17% incorporation of the functional group within the pore system. Continued refluxing is found to reduce the ratio, albeit to a lesser extent than what is observed in the first hour of reaction; however, this is coupled with a consistent increase in percent loading where at 22 h there is 20% incorporation, which increases to 22% by 46 h and finally at 96 h reaches the maximum loading of 25% (Figure S1, Supporting Information). The amount of TPED remaining in solution does not change if the reaction time is extended beyond 96 h, and likewise, the TGA curve indicates that there is no further incorporation of ethylenediamine into the MCM-41 framework.

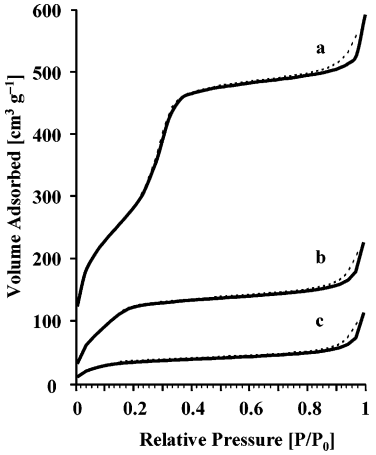

Figure 1. Nitrogen adsorption (—) and desorption (- - -) isotherms for (a) calcined MCM-41, (b) F−MCM-41, and (c) Zn−MCM-41.

Nitrogen adsorption analysis (Figure 1) of this final material confirms maximum loading of ethylenediamine is achieved while a relatively large surface area is maintained and a type IV isotherm is retained. BET analysis indicates that the surface area decreases from 1100 m^2/g for calcined MCM-41 to 480 m^2/g for F−MCM-41 with maximum TPED grafted. As expected, the calculated pore diameter decreases from 3.0 to 2.4 nm, retaining sufficient pore space for further chemical manipulation.

The effect of water on the functionalization process was also investigated by preparing a series of F−MCM-41 materials synthesized with water while maintaining the ratio of MCM-41 to TPED (1:0.25) and varying the ratio of MCM-41 to water from 1:1, 1:0.5, and 1:0.25 and allowing the reactions to reflux for 12 h. The MCM-41:TPED ratio of 1:0.25 was chosen as that material had a significantly large surface area (868 m^2/g) when prepared in the absence of water. In all materials where water was added to increase the population of surface silanol groups, the resulting isotherm did not maintain the type IV isothermal shape as is expected for mesoporous materials.[23] All were found to have smaller surface areas (370−580 m^2/g) in comparison to those of the functionalized materials prepared in the absence of water, where the amount of TPED was varied. Ultimately, it was found that the inclusion of water in the synthesis of F−MCM-41 did not yield materials with greater percent coverage and fundamentally produced materials with dramatically reduced surface areas in which the framework structure could potentially be destroyed. Hence, the study finds

that maximum surface coverage with appreciable surface area can be obtained in the absence of water using a ratio of 1:1 and allowing the reaction to proceed for 96 h.

Synthesis and Characterization of Zn−MCM-41. As silylated chalcogen reagents are readily reactive to both air and water, the use of dry solvents and reagents is required to prevent hydrolysis and oxidation reactions. As such, it is necessary that all MCM-41 materials be dehydrated prior to use and, in particular, the reagents and reactants used in the development of new composite materials be anhydrous in nature. There are several accounts that describe the adsorption of zinc acetate into F−MCM-41; however, these methods use hydrated zinc acetate in aqueous solution.[12a,16d] Anhydrous zinc acetate is efficiently solubilized in chlorinated solvents via the addition of 2.5 equiv of the nitrogen-based ligand, 3,5-lutidine, to quantitatively yield $(3,5\text{-lutidine})_2Zn(OAc)_2$. Introducing a solution of $(3,5\text{-lutidine})_2Zn(OAc)_2$ into F−MCM-41 results in the 3,5-lutidine ligands being displaced from the zinc center and coordination of Zn(II) to the grafted bidentate ethylenediamine moiety. The ligand exchange process is quite rapid in solution as observed by in situ ^{1}H NMR spectroscopy where tetramethylethylenediamine (TMEDA) is chosen as a representative bidentate ligand. The NMR spectrum indicates complete displacement of 3,5-lutidine as noted by the upfield shift in the peak position for the protons associated with free 3,5-lutidine (2.3, 7.3, and 8.3 ppm) versus the proton chemical shifts for complexed 3,5-lutidine (2.4, 7.5, and 8.4 ppm), with coordination of TMEDA to Zn(II). On the basis of TGA of F−MCM-41, there is 25% incorporation of the organic moiety into the mesoporous framework. Given the robustness of the Si−O−Si bonding interaction, it is presumably propylethylenediamine that is lost during thermolysis. Similar functionalized silica materials with aminopropyl groups have been shown to decompose thermally at higher temperatures, where the observed weight loss is attributed to the decomposition of the bonded organic tether.[24] It can be approximated that for every gram of F−MCM-41 there is 2.5 mmol of ethylenediamine encapsulated in MCM-41, and consequently, the maximum loading of zinc acetate will also be 2.5 mmol/g. As the mass of 2.5 mmol of $(3,5\text{-lutidine})_2Zn(OAc)_2$ is 1 g, a 1:1 (m:m) ratio of F−MCM-41 to metal complex will be sufficient to occupy all tethered ethylenediamine moieties.

This incorporation of zinc acetate into the pore structure can be monitored at specified time intervals by both TGA of an isolated solid sample (Figure S2, Supporting Information) and solution ^{1}H NMR spectroscopy of the mother liquor. The optimal reaction time for complete adsorption of zinc acetate can be determined by dissolving $(3,5\text{-lutidine})_2Zn(OAc)_2$ in chloroform-*d* and adding this to a $CDCl_3$ suspension of F−MCM-41. The displacement of 3,5-lutidine from zinc can be monitored by comparing the relative integration of the protons of the acetate groups (6 H) versus the increased amounts of methyl groups of free and coordinated 3,5-lutidine (the latter are not resolved at 400 MHz). Within 30 min of mixing, the degeee of integration of the methyl protons increases by 16%, thus confirming the release of free 3,5-lutidine. This is also reflected by a substantial increase in the extent of loading from that of the parent F−MCM-41 as monitored by TGA (35% vs a value of 25% observed for F−MCM-41). Extending the reaction time leads to both an increase in degree of integration of the methyl substituents and continual incorporation of zinc acetate into the porous structure. The loading capacity noticeably changes while the sample is stirred for 96 h; at 24 h, the percent coverage increases to 38%, while the degree of integration in the ^{1}H NMR spectrum increases by 22%. Maximum zinc incorporation is achieved after the sample has been stirred for 96 h, where surface coverage increases to 44 wt %. These conditions are found to produce a material having a surface area of 130 m^2/g as determined by nitrogen adsorption (Figure 1c).

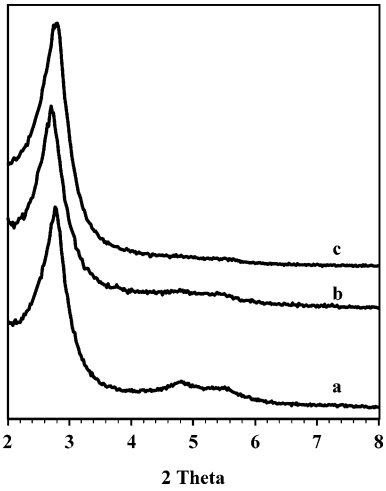

Figure 2. Low-angle powder X-ray diffraction patterns of (a) calcined MCM-41, (b) F−MCM-41, and (c) Zn−MCM-41.

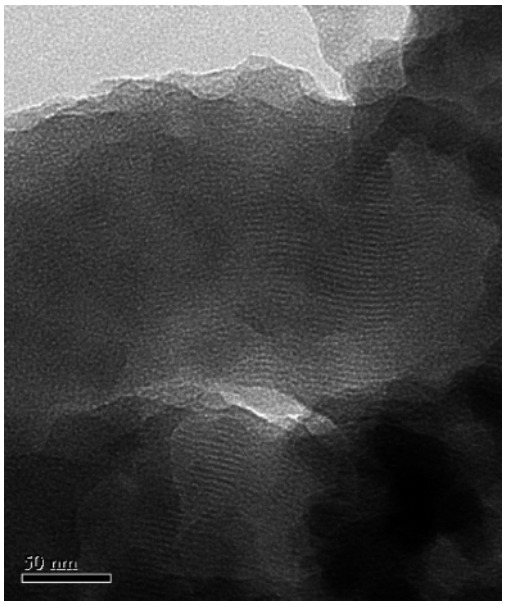

Figure 3. Bright-field TEM image perpendicular to the channel axis of Zn−MCM-41.

The low-angle PXRD patterns for each successive MCM-41 material are shown in Figure 2. Calcined MCM-41 shows three reflections in the PXRD pattern, where the most predominant peak at 2.7° 2θ corresponds to the d_{100} spacing. Both F−MCM-41 and Zn−MCM-41 show retention of the d_{100} reflection, while the two remaining higher-angle peaks are significantly reduced in intensity. Preservation of the d_{100} peak upon sequential functionalization indicates that the hexagonal packing of the mesoporous framework is maintained throughout each synthetic step. The integrity of the porous structure upon formation of Zn−MCM-41 is also confirmed by TEM (Figure 3). The image taken perpendicular to the channel axis indicates that the ordered nature of the channel structure is retained throughout functionalization. In addition, the d_{100} peak shifts to a lower angle with increased surface coverage while decreasing in peak intensity. Typical pore filling is accompanied by a reduction in peak intensity of the composite material in the corresponding PXRD

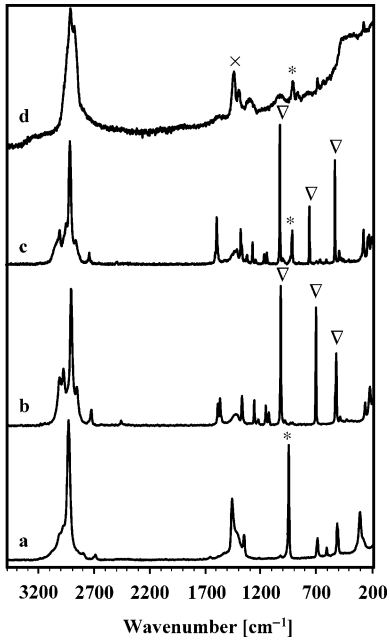

Figure 4. Raman spectra of (a) zinc acetate, (b) 3,5-lutidine, (c) (3,5-lutidine)$_2$Zn(OAc)$_2$, and (d) Zn−MCM-41. C−C bending mode of acetate (*), aromatic ring vibrations of 3,5-lutidine (∇), and C−H deformation of ethylenediamine (×).

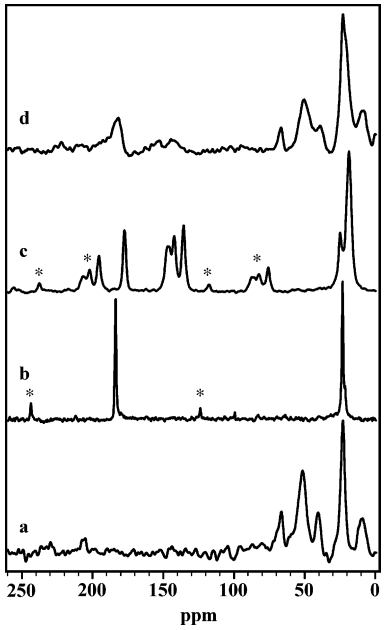

Figure 5. ^{13}C cross-polarization magic-angle spinning (CP MAS) NMR spectra of (a) F−MCM-41, (b) zinc acetate, (c) (3,5-lutidine)$_2$Zn(OAc)$_2$, and (d) Zn−MCM-41. Spinning sidebands are denoted with asterisks.

pattern. This results from a decrease in scattering contrast between the pores and the walls of the mesoporous material upon pore filling. The position of the d_{100} peak is also shifted to lower angles as pore size contracts.[18c,25]

Shown in Figure 4 are Raman spectra of zinc acetate, 3,5-lutidine, and (3,5-lutidine)$_2$Zn(OAc)$_2$. There are two diagnostic Raman bands in the spectrum of zinc acetate, the first a C−C bending mode at 956 cm^{-1} (*) and the second between 2900 and 2800 cm^{-1} due to C−H aliphatic stretching from the methyl groups on the acetate functionality.[26] Both of these bands are retained in the Raman spectrum of (3,5-lutidine)$_2$Zn(OAc)$_2$. The spectrum of 3,5-lutidine (Figure 4b) indicates that aromatic ring vibrations appear at 1034, 716, and 533 cm^{-1} (∇), while aromatic C−H stretching is found between 3100 and 3000 cm^{-1}.[27] These same Raman bands also appear in the spectrum of (3,5-lutidine)$_2$Zn(OAc)$_2$. Loading (3,5-lutidine)$_2$Zn(OAc)$_2$ into F−MCM-41 results in the displacement of 3,5-lutidine and coordination of zinc acetate to the pore wall. This is confirmed in the Raman spectrum of Zn−MCM-41 (Figure 4d) in which there is loss of the Raman bands assigned to 3,5-lutidine and retention of the C−C bending mode from the acetate functionality present on the zinc center.

Raman spectroscopy can also be used to ensure that the organic anchor remains unaltered and thus tethered during the formation of Zn−MCM-41. The Raman spectrum of TPED has only a few Raman active bands (Figure S3, Supporting Information); however, two are diagnostic in determining whether the organic moiety has been attached to the pore wall. The C−H aliphatic stretching band appears between 2900 and 2800 cm^{-1}, and the C−H deformation of the ethylene moiety appears at 1457 cm^{-1} (×).[28] These two bands are retained in the Raman spectra of both F−MCM-41 and Zn−MCM-41 (as noted in Figure 4d for Zn−MCM-41). This suggests that the organic anchor is not destroyed throughout synthetic manipulation; thus, all surface chemistry is occurring within the pore interior, and consequently, the desired binary materials should exhibit quantum confinement effects.

^{13}C CP MAS NMR spectroscopy provides the most direct evidence for identifying chemical species that are present within the pore structure. Shown in Figure 5a is the ^{13}C NMR spectrum of F−MCM-41, which shows the characteristic NMR pattern for propylethylenediamine.[29]

Comparing the ^{13}C CP MAS NMR spectra of zinc acetate and (3,5-lutidine)$_2$Zn(OAc)$_2$ (Figure 5b,c), we find several important similarities and differences. In the NMR spectrum of zinc acetate, there are two chemical shifts observed, one corresponding to the carbonyl carbon (184 ppm) and the other to the methyl carbon of the acetate functionality (24 ppm). The two acetate peaks are also observed in the NMR spectrum of (3,5-lutidine)$_2$Zn(OAc)$_2$; however, the carbonyl peak is shifted slightly upfield to 177 ppm. Also observed are three peaks between 136 and 146 ppm that are assigned to the aromatic carbons of 3,5-lutidine. The methyl substituent on the 3,5-lutidine ring is observed at 19 ppm.

Upon addition of a solution of (3,5-lutidine)$_2$Zn(OAc)$_2$ to F−MCM-41, 3,5-lutidine is displaced as a result of the chelate effect, and this is directly apparent from the ^{13}C CP MAS NMR spectrum of Zn−MCM-41 (Figure 5d). The spectrum confirms the presence of a carbonyl moiety in the material, as evidenced by the peak at 179 ppm. Also, the peak at 24 ppm has increased in intensity as a result of the overlap in the peaks associated with the acetate methyl group and carbon 2 of the propyl chain anchored to the pore wall. There is no evidence of the presence of 3,5-lutidine. This fully supports the proposed synthetic step in which (3,5-lutidine)$_2$Zn(OAc)$_2$ diffuses into the MCM-41 framework, whereby the presence of an anchored chelating ligand favors the exchange of monodentate 3,5-lutidine from the metal center and thus encourages grafting of zinc acetate to the pore surface through the bidentate ligand.

Synthesis and Characterization of ZnE−MCM-41. Generally, metal−chalcogenide materials are formed in MCM-41 by exposing metal salt−MCM-41 composites to H_2E (E = S or Se).[14b−g,15a,16a−e] The use of gaseous reagents can be avoided by otherwise using Na_2S,[14a,i−k,16f] thiourea,[14l] or Na_2SeO_2[15c] as the chalcogen source. An alternative method that has found utility in the formation of binary II−VI and ternary II−II′−VI

nanomaterials is the use of silylated chalcogen reagents.[1,2] Bis(trimethylsilyl) chalcogenides [$E(SiMe_3)_2$] react readily with metal acetates through the liberation of acetoxytrimethylsilane ($AcOSiMe_3$) to yield metal−chalcogenolate complexes with pendant trimethylsilyl moieties.[21,30] The terminal trimethylsilyl group is quite reactive, and in the case of the higher congeners (Se and Te), the corresponding coordination complexes are only stable at relatively low temperatures. Under the appropriate conditions, however, these complexes can further react with a second metal salt to form ternary nanoclusters.[1] By using $E(SiMe_3)_2$ reagents for solid-state surface chemistry, the same reactivity is expected to occur when they are added to metal acetate−MCM-41 complexes, where $AcOSiMe_3$ is generated. Given the propensity of surface silanol groups (even following functionalization) and the unstable nature of the pendant trimethylsilyl group, binary metal−chalcogenide materials can be formed through decomposition within the porous network. Acetoxytrimethylsilane and $E(SiMe_3)_2$ are easily observed by GC−MS, and hence, the formation of zinc−chalcogenide materials within Zn−MCM-41 can be monitored. Generation of the zinc−chalcogenide complexes would be accompanied by the release of $AcOSiMe_3$ in solution paralleled by the consumption of $E(SiMe_3)_2$, leading to the formation of either $Zn-ESiMe_3$ or Zn−E units. This is monitored by adding an internal standard (toluene) to the reaction solution and noting the increase in the ratio of $AcOSiMe_3$ to toluene and, likewise, the decrease in the ratio of $E(SiMe_3)_2$ to toluene over time.

By altering the ratio of Zn−MCM-41 to $S(SiMe_3)_2$, we can determine the optimal quantity of silylated chalcogen needed for complete consumption of the acetate ligand. By using a 1:0.25 Zn−MCM-41:$S(SiMe_3)_2$ ratio (m:v), all of the chalcogen reagent is consumed within the first 30 min whereas small amounts of $S(SiMe_3)_2$ remain after 30 min when a decreased ratio of 1:0.5 is used. If the ratio is decreased to 1:1, a substantial amount of $S(SiMe_3)_2$ remains after 30 min; however, the amount of $AcOSiMe_3$ is only slightly increased from what is observed when using a ratio of 1:0.5. Monitoring these reactions after 2 h, we found that the same amount of $AcOSiMe_3$ is formed in the 1:0.5 reaction and in the 1:1 reaction at 30 min, and no $S(SiMe_3)_2$ remains. Thus, to minimize the use of excess $E(SiMe_3)_2$, a 1:0.5 ratio is ideal for complete conversion of all acetate groups. This ratio is also sufficient for the formation of ZnSe and ZnTe in MCM-41. ZnS−MCM-41 is a colorless solid; ZnSe−MCM-41 is pale yellow in color, while ZnTe−MCM-41 has a red-orange hue. The appearance of color in these samples is a good indication that the desired binary materials are formed. The ZnTe−MCM-41 material is very sensitive to air, and even brief exposure leads to its decomposition.

To understand the formation process that yields binary ZnS within MCM-41, a reaction with a Zn−MCM-41:$S(SiMe_3)_2$ ratio of 1:0.5 is monitored at given time intervals over a period of 160 h. The chalcogen reagent reacts completely within 1 h of stirring, with a negligible amount of $S(SiMe_3)_2$ remaining in solution. With continued stirring, the formation of hexamethyldisiloxane [$O(SiMe_3)_2$] is observed after a 6−17 h time period. The formation of $O(SiMe_3)_2$ reaches a maximum after the sample is stirred for 70 h. During this 70 h period, the quantity of $AcOSiMe_3$ present remains constant; however, after 70 h, $AcOSiMe_3$ starts being consumed, is reduced in amount by just over half by 90 h, and is completely consumed after the sample is stirred for 160 h. It is also noteworthy that when an excess of $S(SiMe_3)_2$ is used the reaction with zinc acetate reaches the same maximum formation of $AcOSiMe_3$ (as the 1:0.5 reaction); however, the amount of excess chalcogen reagent decreases with time, and this is coupled with the generation and continuous increase in the amount of $O(SiMe_3)_2$. The quantity of $O(SiMe_3)_2$ formed is much greater than that in a 1:0.5 reaction mixture and even after the sample is stirred for 160 h does not reach a maximum value as $S(SiMe_3)_2$ still remains in solution. Interestingly, the quantity of $AcOSiMe_3$ remains unchanged through these 160 h for these samples. The similar formation of $AcOSiMe_3$ followed by the generation of $O(SiMe_3)_2$ also occurs in the synthesis of ZnSe and ZnTe in MCM-41, although $O(SiMe_3)_2$ occurs more rapidly than for ZnS. These data have been summarized and can be found in Table S1 of the Supporting Information.

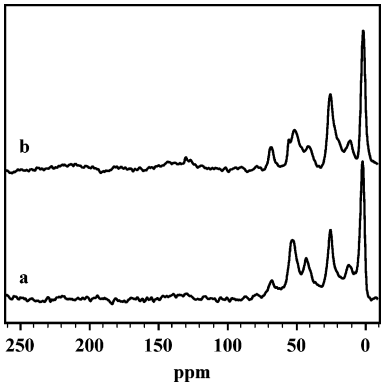

Figure 6. ^{13}C cross-polarization magic-angle spinning (CP MAS) NMR spectra of (a) ZnS−MCM-41 and (b) ZnSe−MCM-41.

^{13}C CP MAS NMR spectra (Figure 6) clearly illustrate the complete reaction of adsorbed zinc acetate with $E(SiMe_3)_2$ as the readily identified carbonyl signal at 179 ppm observed in Zn−MCM-41 is no longer present. In addition, the ^{13}C CP MAS NMR spectra of both ZnS− and ZnSe−MCM-41 display a new peak at 1 ppm. Given both the position and the similarity in chemical shift between the two spectra, this new carbon species is not likely the carbon of a trimethylsilyl−chalcogenolate moiety, as the reported ^{13}C chemical shifts for zinc−trimethylsilyl thiolates and selenolates are ca. 6 ppm.[21] This substantiates the proposed mechanism in which any pendant trimethylsilyl groups generated within MCM-41 decompose hydrolytically and/or thermolytically to form ZnE materials in the pores.

The formation of $O(SiMe_3)_2$ supports the pathway to the formation of ZnE materials. On the basis of the GC study, an excess of $S(SiMe_3)_2$ is found to gradually decompose within the porous structure, yielding $O(SiMe_3)_2$; however, $S(SiMe_3)_2$ reacts preferentially with $Zn(OAc)_2$ upon addition to Zn−MCM-41, as $AcOSiMe_3$ is the first byproduct to be formed. Hexamethyldisiloxane is generated through a self-condensation reaction between 2 equiv of Me_3SiOH,[31] where Me_3SiOH can only be formed from hydrolysis of $S(SiMe_3)_2$, with the concomitant formation of H_2S. This same hydrolysis mechanism is expected to occur for $Se(SiMe_3)_2$ and $Te(SiMe_3)_2$. Water needed to facilitate this reaction would come from a residual amount of chemisorbed water on the mesoporous surface, which is not removed under the designated dehydration conditions of F−MCM-41. The presence of zinc acetate ensures the preferential reactivity of $E(SiMe_3)_2$ at the metal center; hence, no $O(SiMe_3)_2$ is formed within the first several hours of stirring. The general reactivity and lability of any formed terminal trimethylsilyl chalcogenolate ligands bound to zinc (vs zinc−chalcogenide complexes) leads to rapid decomposition of the zinc complex, especially for the selenolate and tellurolate complexes given the room-temperature nature of this reaction.

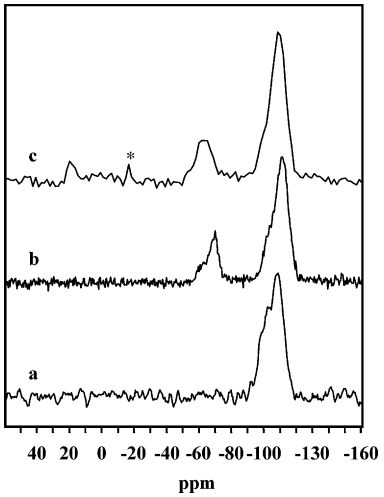

Figure 7. ^{29}Si magic-angle spinning (MAS) spectra of (a) calcined MCM-41, (b) F−MCM-41, and (c) ZnS−MCM-41. Silicon grease is denoted with an asterisk.

It is presumed that the zinc complex decomposes to form $E(SiMe_3)_2$ which further undergoes hydrolysis to generate $O(SiMe_3)_2$.

Throughout the hydrolysis of $E(SiMe_3)_2$, acetoxytrimethylsilane persists in the reaction solution and is only consumed when no $E(SiMe_3)_2$ remains in solution. This again indicates preferential reactivity within MCM-41 where initially silylated chalcogen reagents react with zinc acetate, followed by hydrolysis of the remaining $E(SiMe_3)_2$ and completed with the reactivity of $AcOSiMe_3$. It has been shown that $AcOSiMe_3$ reacts with surface silanol groups to form trimethylsilyl moieties on the surface of a silica framework.[32] Thus, the peaks observed at ∼1 ppm in the ^{13}C CP MAS NMR spectra of both ZnS and ZnSe−MCM-41 are consistent with a surface trimethylsilyl group. The formation of a trimethylsilyl group is also identified using ^{29}Si MAS NMR spectroscopy (Figure 7). Framework silicon atoms are observed upfield in the ^{29}Si MAS NMR spectrum for calcined MCM-41. The chemical shift at −106 ppm is in accordance with the expected chemical shift for $(SiO_3)SiOH$ (Q^3 silicon species). Upon functionalization of MCM-41 (Figure 7b), the chemical shift associated with framework silicon is further shifted upfield to −112 ppm, thus reflecting the conversion of Q^3 sites to Q^4 sites [$(SiO_4)Si$] as a result of functionalization. In addition, the silicon atom attached to the propylethylenediamine fragment appears downfield at −70 ppm. The ^{29}Si MAS NMR spectrum of ZnS−MCM-41 (Figure 7c) indicates a third silicon species within the porous framework at 17 ppm. The occurrence of this chemical shift confirms the formation of surface trimethylsilyl fragments.

The nitrogen adsorption isotherms for ZnS and ZnSe−MCM-41 are shown in Figure 8. Like the shape of the nitrogen adsorption isotherm of Zn−MCM-41, the shape of the type IV isotherm is no longer present when the pore is filled with ZnE materials. The BET surface area decreases only slightly upon inclusion of the binary material, changing from 130 m^2/g as observed for Zn−MCM-41 to 115 and 103 m^2/g for ZnS and ZnSe−MCM-41, respectively. Despite the small surface area, the PXRD patterns for each of these materials (not shown) retain the d_{100} peak, although shifted below 2° 2θ.

The formation of the ZnE−MCM-41 complex is confirmed by EDX analysis and UV−vis spectroscopy. To ensure reproducibility, EDX analysis was performed on three different areas of the sample and the average of the three analyses (using atomic percentages) was used in determining the overall ratio. ZnS−MCM-41 has a ratio of 1:1.02 (Zn:S), ZnSe−MCM-41 a ratio of 1:1.2 (Zn:Se), and ZnTe−MCM-41 a ratio of 1:0.92 (Zn:Te), in agreement with the expected 1:1 ratio for ZnE materials.

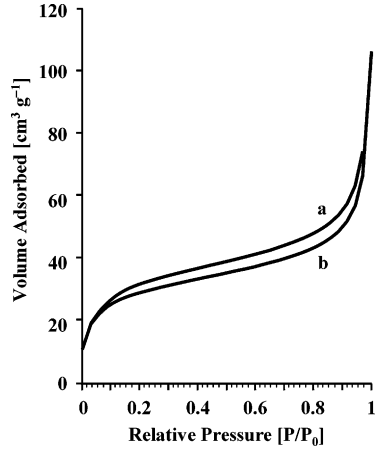

Figure 8. Nitrogen adsorption isotherms of (a) ZnS−MCM-41 and (b) ZnSe−MCM-41.

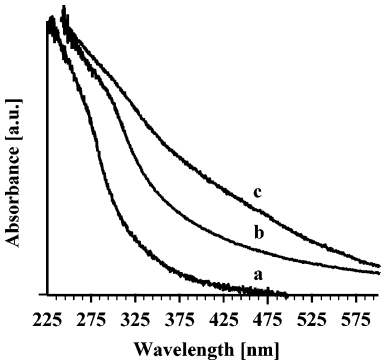

Figure 9. UV−vis absorption spectra of (a) ZnS−MCM-41, (b) ZnSe−MCM-41, and (c) ZnTe−MCM-41.

The UV−vis absorption spectra of ZnS and ZnSe−MCM-41 are shown in Figure 9. The samples display poorly resolved absorption maxima at 260 nm (4.77 eV) and 290 nm (4.28 eV) for ZnS and ZnSe−MCM-41, respectively (Figure 9a,b). The absorption peak for ZnS−MCM-41 is at a higher energy than that observed for pre-prepared ∼2.2 nm ZnS nanoparticles loaded into MCM-41[33] and is consistent with the formation of much smaller clusters here.[34] The onset of absorption occurs at 300 nm for ZnS−MCM-41 which suggests a broad distribution of particle sizes. In all cases, however, these absorption spectra indicate that the maximum absorbance for encapsulated zinc−chalcogenide complexes is blue shifted from the respective parent semiconductor material, where bulk ZnS absorbs at 337 nm (3.68 eV) and bulk ZnSe absorbs at 461 nm (2.69 eV).[35] Due to the moisture sensitive nature of ZnTe, obtaining a UV−vis spectrum of ZnTe−MCM-41 is more difficult as ZnTe−MCM-41 is oxidized during the analysis period; however, dried mineral oil can be used as a matrix in obtaining an absorption spectrum of ZnTe. The absorption maximum (Figure 9c) of ZnTe−MCM-41 is red shifted (306 nm, 3.26 eV) versus the lighter chalcogenides but blue shifted relative to bulk ZnTe (544 nm, 2.28 eV).[35] Luminescence spectra of ZnSe−MCM-41 display only weak emission, with a red-shifted, broad peak centered at 440 nm.

Conclusions

Silylated chalcogen reagents have been proven to be efficient delivery sources of E^{2-} in the pursuit of binary zinc chalco-

genides within MCM-41. The composites investigated in this study are the first metal chalcogenide materials encapsulated in a mesoporous environment that have been synthesized using this approach. Thermolysis of the solid sample after solution loading is not required for the formation of the desired binary materials as all chemistry occurs on the surface of MCM-41 at room temperature. Moreover, this is the first account of ZnSe and ZnTe formation in MCM−41. The apparent blue shift in the absorption maximum from the bulk material indicates that ZnE materials incorporated in the framework display characteristic quantum confinement effects. The success in using $E(SiMe_3)_2$ in the formation of ZnE materials in MCM-41 suggests that this method could also be a viable route to accessing CdE and possibly HgE materials in a mesoporous environment.

Acknowledgment. We gratefully acknowledge the Natural Sciences and Engineering Research Council (NSERC) of Canada for financial support of this research, equipment funding, and a postgraduate scholarship (E.A.T.). The Government of Ontario Premier's Research Excellence Awards (PREA) program is also acknowledged for financial support, and The University of Western Ontario and the Canada Foundation for Innovation (CFI) are thanked for equipment funding. J.F.C. also thanks the Forschungszentrum Karlsruhe for a visiting research fellowship.

Supporting Information Available: Raman spectra for TPED and F−MCM-41 and thermogravimetric analysis (TGA) curves for F−MCM-41 and Zn−MCM-41 collected over the reaction period. This material is available free of charge via the Internet at http://pubs.acs.org.

References and Notes

(1) Corrigan, J. F.; Balter, S.; Fenske, D. *J. Chem. Soc., Dalton Trans.* **1996**, 729−738. (b) Corrigan, J. F.; Fenske, D. *Chem. Commun.* **1997**, 1837−1838. (c) Tran, D. T. T.; Taylor, N. J.; Corrigan, J. F. *Angew. Chem., Int. Ed.* **2000**, *39*, 935−937. (d) Lorenz, A.; Fenske, D. *Angew. Chem., Int. Ed.* **2001**, *40*, 4402−4406. (e) Wallbank, A. I.; Corrigan, J. F. *Chem. Commun.* **2001**, 377−378. (f) Lebold, T. P.; Stringle, D. L. B.; Workentin, M. S.; Corrigan, J. F. *Chem. Commun.* **2003**, 1398−1399. (g) Olkowska-Oetzel, J.; Sevillano, P.; Eichhöfer, A.; Fenske, D. *Eur. J. Inorg. Chem.* **2004**, 1100−1106. (h) DeGroot, M. W.; Taylor, N. J.; Corrigan, J. F. *Inorg. Chem.* **2005**, *44*, 5447−5458.

(2) Steigerwald, M. L.; Alivisatos, A. P.; Gibson, J. M.; Harris, T. D.; Kortan, A. R.; Muller, A. J.; Thayer, A. M.; Duncan, T. M.; Douglass, D. C.; Brus, L. E. *J. Am. Chem. Soc.* **1988**, *110*, 3046−3050. (b) Stuczynski, S. M.; Brennan, J. G.; Steigerwald, M. L. *Inorg. Chem.* **1989**, *28*, 4431−4432. (c) Kortan, A. R.; Hull, R.; Opila, R. L.; Bawendi, M. G.; Steigerwald, M. L.; Carrol, P. J.; Brus, L. E. *J. Am. Chem. Soc.* **1990**, *112*, 1327−1332. (d) Murray, C. B.; Norris, D. J.; Bawendi, M. G. *J. Am. Chem. Soc.* **1993**, *115*, 8706−8715.

(3) DeGroot, M. W.; Corrigan, J. F. In *Comprehensive Coordination Chemistry II*; Fujita, M., Powell, A., Creutz, C., Eds.; Pergamon: Oxford, U.K., 2004; Vol. 7, pp 57−123.

(4) Kresge, C. T.; Leonowicz, M. E.; Roth, W. J.; Vartuli, J. C.; Beck, J. S. *Nature* **1992**, *359*, 710−712. (b) Beck, J. S.; Vartuli, J. C.; Roth, W. J.; Leonowicz, M. E.; Kresge, C. T.; Schmitt, K. D.; Chu, C. T.-W.; Olson, D. H.; Sheppard, E. W.; McCullen, S. B.; Higgins, J. B.; Schlenker, J. L. *J. Am. Chem. Soc.* **1992**, *114*, 10834−10843.

(5) Zhao, D.; Feng, J.; Huo, Q.; Melosh, N.; Fredrickson, G. H.; Chmelka, B. F.; Stucky, G. D. *Science* **1998**, *279*, 548−552. (b) Zhao, D.; Huo, Q.; Feng, J.; Chmelka, B. F.; Stucky, G. D. *J. Am. Chem. Soc.* **1998**, *120*, 6024−6036.

(6) Sayari, A. *Chem. Mater.* **1996**, *8*, 1840−1852. (b) Corma, A. *Top. Catal.* **1997**, *4*, 249−260. (c) Schüth, F.; Wingen, A.; Sauer, J. *Microporous Mesoporous Mater.* **2001**, *44*−*45*, 465−476.

(7) Tajima, K.; Aida, T. *Chem. Commun.* **2000**, 2399−2412. (b) Showkat, A. M.; Lee, K.-P.; Gopalan, A. I.; Kim, M.-S.; Choi, S.-H.; Kang, H.-D. *Polymer* **2005**, *46*, 1804−1812. (c) Choi, M.; Kleitz, F.; Liu, D.; Lee, H. Y.; Ahn, W.-S.; Ryoo, R. *J. Am. Chem. Soc.* **2005**, *127*, 1924−1932.

(8) Kisler, J. M.; Dähler, A.; Stevens, G. W.; O'Connor, A. J. *Microporous Mesoporous Mater.* **2001**, *44*−*45*, 769−774. (b) Shiraishi, Y.; Nishimura, G.; Hirai, T.; Komasawa, I. *Ind. Eng. Chem. Res.* **2002**, *41*, 5065−5070. (c) Newalkar, B. L.; Choudary, N. V.; Kumar, P.; Komarneni, S.; Bhat, T. S. G. *Chem. Mater.* **2002**, *14*, 304−309.

(9) Coleman, N. R. B.; Morris, M. A.; Spalding, T. R.; Holmes, J. D. *J. Am. Chem. Soc.* **2001**, *123*, 187−188.

(10) Leon, R.; Margolese, D.; Stucky, G.; Petroff, P. M. *Phys. Rev. B* **1995**, *52*, R2285−R2288.

(11) Srdanov, V. I.; Alxneit, I.; Stucky, G. D.; Reaves, C. M.; DenBaars, S. P. *J. Phys. Chem. B* **1998**, *102*, 3341−3344. (b) Winkler, H.; Birkner, A.; Hagen, V.; Wolf, I.; Schmechel, R.; von Seggern, H.; Fischer, R. A. *Adv. Mater.* **1999**, *11*, 1444−1448. (c) Su, J.; Cui, G.; Gherasimova, M.; Tsukamoto, H.; Han, J.; Ciuparu, D.; Lim, S.; Pfefferle, L.; He, Y.; Nurmikko, A. V.; Broadbridge, C.; Lehman, A. *Appl. Phys. Lett.* **2005**, *86*, 013105-1−013105-3. (d) Agger, J. R.; Anderson, M. W.; Pemble, M. E.; Terasaki, O.; Nozue, Y. *J. Phys. Chem. B* **1998**, *102*, 3345−3353.

(12) Zhang, W.-H.; Shi, J.-L.; Wang, L.-Z.; Yan, D.-S. *Chem. Mater.* **2000**, *12*, 1408−1413. (b) Dappurkar, S. E.; Badamali, S. K.; Selvam, P. *Catal. Today* **2001**, *68*, 63−68. (c) Lu, W.; Lu, G.; Luo, Y.; Chen, A. *J. Mol. Catal. A: Chem.* **2002**, *188*, 225−231. (d) Crowley, T. A.; Ziegler, K. J.; Lyons, D. M.; Erts, D.; Olin, H.; Morris, M. A.; Holmes, J. D. *Chem. Mater.* **2003**, *15*, 3518−3522. (e) Guari, Y.; Soulantica, K.; Philippot, K.; Thieuleux, C.; Mehdi, A.; Reyé, C.; Chaudret, B.; Corriu, R. J. P. *New J. Chem.* **2003**, *27*, 1029−1031. (f) Guo, H.; Xu, W.; Cui, M.-H.; Yang, N.-L.; Akins, D. L. *Chem. Commun.* **2003**, 1432−1433. (g) Vetrivel, S.; Pandurangan, A. *Ind. Eng. Chem. Res.* **2005**, *44*, 692−701.

(13) Zhao, X.-G.; Shi, J.-L.; Hu, B.; Zhang, L.-X.; Hua, Z.-L. *J. Mater. Chem.* **2003**, *13*, 399−403.

(14) Chen, W.; Xu, Y.; Lin, Z.; Wang, Z.; Lin, L. *Solid State Commun.* **1998**, *105*, 129−134. (b) Chen, L.; Klar, P. J.; Heimbrodt, W.; Brieler, F.; Fröba, M. *Appl. Phys. Lett.* **2000**, *76*, 3531−3533. (c) Chen, L.; Klar, P. J.; Heimbrodt, W.; Brieler, F.; Fröba, M.; Krug von Nidda, H.-A.; Loidl, A. *Physica E* **2001**, *10*, 368−372. (d) Brieler, F. J.; Fröba, M.; Chen, L.; Klar, P. J.; Heimbrodt, W.; Krug von Nidda, H.-A.; Loidl, A. *Chem.*−*Eur. J.* **2002**, *8*, 185−194. (e) Brieler, F. J.; Grundmann, P.; Fröba, M.; Chen, L.; Klar, P. J.; Heimbrodt, W.; Krug von Nidda, H.-A.; Kurz, T.; Loidl, A. *Chem. Mater.* **2005**, *17*, 795−803. (f) Wellmann, H.; Rathousky, J.; Wark, M.; Zukal, A.; Schulz-Ekloff, G. *Microporous Mesoporous Mater.* **2001**, *44*−*45*, 419−425. (g) Xu, W.; Liao, Y.; Akins, D. L. *J. Phys. Chem. B* **2002**, *106*, 11127−11131. (h) Gao, F.; Lu, Q.; Zhao, D. *Chem. Phys. Lett.* **2002**, *360*, 585−591. (i) Hirai, T.; Okubo, H.; Komasawa, I. *J. Phys. Chem. B* **1999**, *103*, 4228−4230. (j) Hirai, T.; Okubo, H.; Komasawa, I. *J. Colloid Interface Sci.* **2001**, *235*, 358−364. (k) Chae, W.-S.; Ko, J.-H.; Hwang, I.-W.; Kim, Y.-R. *Chem. Phys. Lett.* **2002**, *365*, 49−56. (l) Liu, X.; Tian, B.; Yu, C.; Tu, B.; Liu, Z.; Terasaki, O.; Zhao, D. *Chem. Lett.* **2003**, *32*, 824−825.

(15) Chen, L.; Falk, H.; Klar, P. J.; Heimbrodt, W.; Brieler, F.; Fröba, M.; Krug von Nidda, H.-A.; Loidl, A.; Chen, Z.; Oka, Y. *Phys. Status Solidi B* **2002**, *229*, 31−34. (b) Parala, H.; Winkler, H.; Kolbe, M.; Wohlfart, A.; Fischer, R. A.; Schmechel, R.; von Seggern, H. *Adv. Mater.* **2000**, *12*, 1050−1055. (c) Shan, Y.; Gao, L.; Zheng, S. *Mater. Chem. Phys.* **2004**, *88*, 192−196.

(16) Chen, L.; Klar, P. J.; Heimbrodt, W.; Brieler, F. J.; Fröba, M.; Krug von Nidda, H.-A.; Kurz, T.; Loidl, A. *J. Appl. Phys.* **2003**, *93*, 1326−1328. (b) Chen, L.; Klar, P. J.; Heimbrodt, W.; Brieler, F. J.; Fröba, M. *J. Supercond.* **2003**, *16*, 99−102. (c) Brieler, F. J.; Grundmann, P.; Fröba, M.; Chen, L.; Klar, P. J.; Heimbrodt, W.; Krug von Nidda, H.-A.; Kurz, T.; Loidl, A. *J. Am. Chem. Soc.* **2004**, *126*, 797−807. (d) Zhang, W.-H.; Shi, J.-L.; Chen, H.-R.; Hua, Z.-L.; Yan, D.-S. *Chem. Mater.* **2001**, *13*, 648−654. (e) Xi, H.; Qian, X.; Yin, J.; Bian, L.; He, R.; Zhu, Z. *Mater. Lett.* **2003**, *57*, 2657−2661. (f) Chae, W.-S.; Yoon, J.-H.; Yu, H.; Jang, D.-J.; Kim, Y.-R. *J. Phys. Chem. B* **2004**, *108*, 11509−11513.

(17) a) Turner, E. A.; Huang, Y.; Corrigan, J. F. *Eur. J. Inorg. Chem.* **2005**, 4465−4478. (b) Brieler, F. J.; Grundmann, P.; Fröba, M.; Chen, L.; Klar, P. J.; Heimbrodt, W.; Krug von Nidda, H.-A.; Kurz, T.; Loidl, A. *Eur. J. Inorg. Chem.* **2005**, 3597−3611.

(18) Stein, A.; Melde, B. J.; Schroden, R. C. *Adv. Mater.* **2000**, *12*, 1403−1419. (b) Sayari, A.; Hamoudi, S. *Chem. Mater.* **2001**, *13*, 3151−3168. (c) Lim, M. H.; Stein, A. *Chem. Mater.* **1999**, *11*, 3285−3295. (d) Asefa, T.; MacLachlan, M. J.; Coombs, N.; Ozin, G. A. *Nature* **1999**, *402*, 867−871. (e) Igarashi, N.; Hashimoto, K.; Tatsumi, T. *J. Mater. Chem.* **2002**, *12*, 3631−3636. (f) Jia, M.; Seifert, A.; Berger, M.; Giegengack, H.; Schulze, S.; Thiel, W. R. *Chem. Mater.* **2004**, *16*, 877−882. (g) Cauvel, A.; Renard, G.; Brunel, D. *J. Org. Chem.* **1997**, *62*, 749−751. (h) Choudary, B. M.; Lakshmi Kantam, M.; Sreekanth, P.; Bandopadhyay, T.; Figueras, F.; Tuel, A. *J. Mol. Catal. A: Chem.* **1999**, *142*, 361−365. (i) Nunes, C. D.; Valente, A. A.; Pillinger, M.; Fernandes, A. C.; Romão, C. C.; Rocha, J.; Gonçalves, I. S. *J. Mater. Chem.* **2002**, *12*, 1735−1742. (j) Alvaro, M.; Corma, A.; Das, D.; Fornés, V.; García, H. *J. Catal.* **2005**, *231*, 48−55.

(19) Pangborn, A. B.; Giardello, M. A.; Grubbs, R. H.; Rosen, R. K.; Timmers, F. J. *Organometallics* **1996**, *15*, 1518−1520.

(20) So, J.-H.; Boudjouk, P. *Synthesis* **1989**, 306−307. (b) DeGroot, M. W.; Taylor, N. J.; Corrigan, J. F. *J. Mater. Chem.* **2004**, *14*, 654−660.

(21) DeGroot, M. W.; Corrigan, J. F. *Organometallics* **2005**, *24*, 3378−3385.

(22) Feng, X.; Fryxell, G. E.; Wang, L.-Q.; Kim, A. Y.; Liu, J.; Kemner, K. M. *Science* **1997**, *276*, 923−926.

(23) Sing, K. S. W.; Everett, D. H.; Haul, R. A. W.; Moscou, L.; Pierotti, R. A.; Rouquérol, J.; Siemieniewska, T. *Pure Appl. Chem.* **1985**, *57*, 603−619.

(24) Jaroniec, C. P.; Gilpin, R. K.; Jaroniec, M. *J. Phys. Chem. B* **1997**, *101*, 6861−6866. (b) Jaroniec, C. P.; Kruk, M.; Jaroniec, M.; Sayari, A. *J. Phys. Chem. B* **1998**, *102*, 5503−5510. (c) Antochshuk, V.; Jaroniec, M. *Chem. Mater.* **2000**, *12*, 2496−2501. (d) Olkhovyk, O.; Antochshuk, V.; Jaroniec, M. *Analyst* **2005**, *130*, 104−108.

(25) Burkett, S. L.; Sims, S. D.; Mann, S. *Chem. Commun.* **1996**, 1367−1368. (b) Marler, B.; Oberhagemann, U.; Vortmann, S.; Gies, H. *Microporous Mater.* **1996**, *6*, 375−383. (c) Fowler, C. E.; Burkett, S. L.; Mann, S. *Chem. Commun.* **1997**, 1769−1770.

(26) Ishioka, T.; Shibata, Y.; Takahashi, M.; Kanesaka, I. *Spectrochim. Acta, Part A* **1998**, *54*, 1811−1818.

(27) Yurdakul, S.; Akyüz, S.; Davies, J. E. D. *Synth. React. Inorg. Met.* **1997**, *27*, 1235−1248. (b) Arenas, J. F.; López Tocón, I.; Otero, J. C.; Marcos, J. I. *J. Mol. Struct.* **1999**, *476*, 139−150. (c) Green, J. H. S.; Harrison, D. J.; Kynaston, W.; Paisley, H. M. *Spectrochim. Acta, Part A* **1970**, *26*, 2139−2146.

(28) Diot, A.; Theophanides, T. *Can. J. Spectrosc.* **1972**, *17*, 67−72.

(29) Chiang, C. H.; Liu, N.-I.; Koenig, J. L. *J. Colloid Interface Sci.* **1982**, *86*, 26−34.

(30) Tran, D. T. T.; Corrigan, J. F. *Organometallics* **2000**, *19*, 5202−5208. (b) DeGroot, M. W.; Taylor, N. J.; Corrigan, J. F. *J. Am. Chem. Soc.* **2003**, *125*, 864−865. (c) DeGroot, M. W.; Corrigan, J. F. *Angew. Chem., Int. Ed.* **2004**, *43*, 5355−5357.

(31) Grubb, W. T. *J. Am. Chem. Soc.* **1954**, *76*, 3408−3414. (b) Cella, J. A.; Carpenter, J. C. *J. Organomet. Chem.* **1994**, *480*, 23−26.

(32) Hideki, K.; Masayuki, O. European Patent 0251176B1, 1992.

(33) Zhang, J.; Han, B.; Hou, Z.; Liu, Z.; He, J.; Jiang, T. *Langmuir* **2003**, *19*, 7616−7620.

(34) Bertoncello, R.; Bettinelli, M.; Casarin, M.; Maccato, C.; Pandolfo, L.; Vittadini, A. *Inorg. Chem.* **1997**, *36*, 4707−4716. (b) Han, J. G.; Li, J. Q.; He, T.-J.; Liu, F.-C.; Zhang, Y.-W. *THEOCHEM* **1995**, *331*, 249−253.

(35) *Semiconductors Basic Data*, 2nd ed.; Madelung, O., Ed.; Springer: Berlin, 1996. (b) Adachi, S. *Optical Constants of Crystalline and Amorphous Semiconductors: Numerical Data and Graphical Information*; Kluwer Academic Publishers: Boston, 1999; pp 445−477.